JOURNAL OF CATALYSIS **179,** 420–430 (1998)
ARTICLE NO. CA982232

OH Gas Phase Chemistry outside a Pt Catalyst

F. Gudmundson,* J. L. Persson,* M. Försth,*,[1] F. Behrendt,† B. Kasemo,‡ and A. Rosén*

*Department of Experimental Physics, ‡Department of Applied Physics, Chalmers University of Technology and Göteborg University, S-412 96 Göteborg, Sweden; †Universität Heidelberg, Interdisziplinäres Zentrum für Wissenschaftliches Rechnen, Im Neuenheimer Feld 386, D-691 20 Heidelberg, Germany

Received February 5, 1998; revised July 14, 1998; accepted July 14, 1998

Using planar laser induced fluorescence we have measured the OH concentration profiles outside a Pt catalyst at 1, 5, and 10 torr. The catalyst was heated to 1300 K in a stagnation point flow consisting of 10% hydrogen and 90% oxygen directed onto the surface. The measurements were compared to a model describing a laminar stagnation point flow including a detailed mechanism with elementary reactions in order to describe both the gas phase and surface reactions. The simulation shows that the detected OH was not produced by gas phase reactions. Instead it is formed on the surface by $H + O$ recombination, and a small percentage of it desorbs and diffuses out from the catalyst. At 1 torr the form of the OH gradient outside the catalyst was found to be determined solely by diffusion and convection. At 5 and 10 torr gas phase reactions also had to be included to correctly describe the shape of the OH concentration gradient. The dominant gas phase reaction is removal of OH molecules through reaction with hydrogen. © 1998 Academic Press

---

INTRODUCTION

The coupling of surface and gas phase chemistry is a central issue in processes like catalytic combustion, ignition, and combustion near surfaces (1, 2). Another emerging field, where the connection between surface and gas phase reactions is essential, is when surface and gas phase reactions are combined to produce desired chemicals as, for example, in the oxidative coupling of methane or in chemical vapor deposition of surface coatings (3, 4). Catalytic combustion of a gaseous fuel on and outside a catalyst can be either purely catalytic, i.e. with no gas phase reactions, or based on combined catalytic and gas phase reactions. Both types of reaction—heterogeneous and homogeneous—are quite complex alone, and even more complex in combination. Better understanding of the relative importance of phenomena, like the inclusion of of backward reactions on the surfaces, radical recombination on surfaces, enhanced gas phase kinetics, and ignition by desorbed radicals, is required to improve and optimize catalytic combustion techniques. Ignition and combustion phenomena near surfaces are also of key interest in the design of combustion engines.

Coupled surface and gas phase kinetics require pressures where the mean-free path for molecular collisions in the gas phase allows many gas phase collisions, i.e. pressures $>10^{-2}$ torr, which correspond to a mean-free path of some centimeters or less. Clearly it is of interest to study the relative importance of surface and gas phase kinetics, at different pressures. This requires both experimental and theoretical/simulation work. It is necessary to develop relevant experimental techniques, as well as reliable computer models that describe the combined system of both surface and gas phase reactions, including mass and heat transport. Such models should first be developed and tested in simple geometries, and with simple reactions with well-known mechanisms in the individual surface and gas phase cases, before more complex geometries (e.g., monolith) and complex reactions (longer hydrocarbons) are addressed.

The $H_2 + O_2$ reaction on Pt and in the gas phase constitutes one of the best known model systems for such model studies. For this case we address the situation by experimental measurements and simulations of surface and gas phase chemistry in a stagnation flow. The chosen model system has several advantages. One of the most important is the existence of computer models, including full surface and gas phase chemistry for stagnation flow. The gas phase chemistry is well known (5) and the surface mechanism for the water formation reaction has been studied extensively (6, with a number of references therein). The model describing the water formation on platinum has been qualitatively validated for a large range of parameters, including the high temperature regime at low pressures where the influence of the gas phase chemistry is small or of no importance (7–16). This model has also been successfully used to describe catalytic ignition temperatures of different hydrogen–oxygen mixtures in a carrier gas at ambient pressure (17). Thus both the surface and gas phase reaction mechanisms have been validated in separate studies.

We have in this work performed a combined experimental and numerical study of the $H_2 + O_2$ reaction outside a Pt surface at 1300 K in the pressure range 1 to 10 torr. In the experiment the concentration and temperature profiles of OH are measured outside the surface. The temperature

---

[1] Corresponding author. E-mail: forsth@fy.chalmers.se.

0021-9517/98 $25.00

profiles are used as input in the numerical simulations which combine a surface kinetics scheme, a gas phase kinetics scheme, and mass transport. The calculated OH concentration profiles outside the surface are compared with the experimental results.

We have earlier in a number of works studied the yield of OH from polycrystalline Pt foils and single crystal Pt(111) surfaces in the temperature range 900–1300 K and pressures up to 200 mtorr (7–16). In this work we especially address the question at what pressures gas phase chemistry begins to play an important role and at what pressures the surface reactions dominate. We also present data on the relative importance of different reaction paths involved in the chemistry induced by surface-desorbed OH. In the next paragraph we discuss the complications that have to be considered when the coupled gas-surface chemistry is modeled and how these problems have been addressed by others.

We are currently working on extending these studies to higher pressures, where gas phase reactions become increasingly more important (18).

COUPLING OF SURFACE AND GAS CHEMISTRY IN LAMINAR FLOW REGIME

The experiments in this work as described in detail in the next section are focussed on studies of the concentration and temperature of OH radicals outside a catalytic Pt foil at various pressures. The crucial issues in these experimental studies and in the kinetic modeling are how the measured OH has been produced from the surface and/or from reactions in the gas phase. Two different, more complete mechanisms for the formation of water on platinum surfaces have been presented by Hellsing *et al.* (6) and by Antogan and Cadogan (19). These models differ in describing the process from adsorbed atomic hydrogen and oxygen to adsorbed water molecules. Below we will briefly summarize the model for hydrogen oxidation on a Pt surface developed by Hellsing *et al.* (6, 8, 15) which is the mechanism used in this work. The full reaction schemes for both the surface and gas chemistry are given in the Methods section below. The assumed reaction scheme for the process is the following:

$$\begin{aligned} \mathrm{H_2} &\leftrightarrow \mathrm{2H(s)} \\ \mathrm{O_2} &\leftrightarrow \mathrm{2O(s)} \\ \mathrm{H(s)+O(s)} &\leftrightarrow \mathrm{OH(s)} \\ \mathrm{H(s)+OH(s)} &\leftrightarrow \mathrm{H_2O(s)} \leftrightarrow \mathrm{H_2O}, \end{aligned}$$

where an (s) means the molecule is adsorbed on the surface. No (s) means that the molecule is in the gas phase. The hydrogen addition path is the dominant one at high temperature, whereas the hydroxyl disproportionation path:

$$\mathrm{2OH(s)} \leftrightarrow \mathrm{O(s)} + \mathrm{H_2O(s)} \leftrightarrow \mathrm{H_2O}$$

has been demonstrated to be the low temperature path (6). At sufficiently high temperatures the intermediate OH(s) may desorb before it reacts to form water. This is the minority path which is responsible for the desorbed OH that can be detected by LIF.

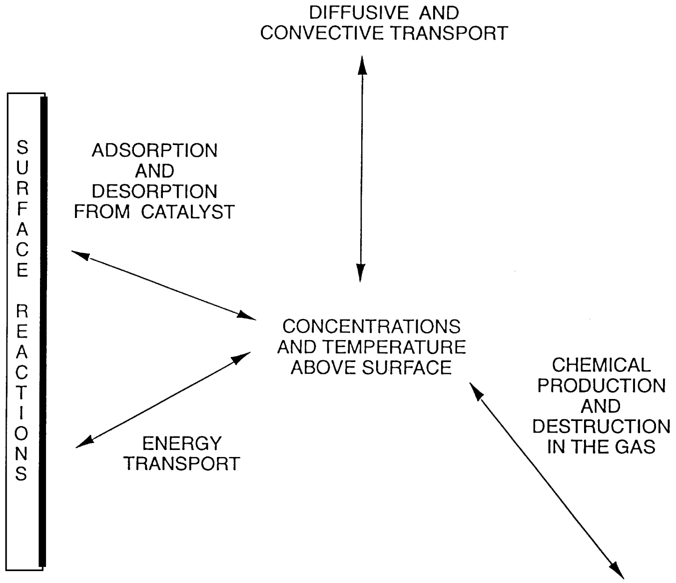

FIG. 1. Schematic picture of gas surface interaction to be taken into account when modeling catalysis in a laminar flow.

Going from low pressure experiments in the molecular flow regime, where the process is dominated by the surface reactions to higher pressures where viscous flow prevails, a number of phenomena have to be considered. Some of them are presented in Fig. 1. They are listed below and further discussed in the subsequent text.

- change of gas phase composition near the surface because of gradients that are created when the diffusive transport constant matches the rate of convection at the surface
- re-adsorption of products and desorbed intermediates
- adsorbate–adsorbate interactions at higher coverages which may change the rate constants of the surface processes, compared to the low coverage case
- increased gas phase reactivity due to desorption of radicals from the surface formed as intermediates in the catalytic reaction.

The surface may also alter the reaction conditions in the gas phase outside the surface via some of the following phenomena:

- decreased gas phase reactivity due to adsorption of radicals produced by gas phase reactions
- increased/decreased gas phase reactivity due to the heat transfer to or from the surface
- catalytic consumption of reactants which may suppress gas phase reactivity near the surface.

If the catalytic reaction is very efficient it will cause a change in the gas composition at the surface because of mass transport limitations; i.e. concentration gradients are established. The extent to which the gas composition is changed near the surface depends on the balance between reaction rate and transport. The predominant transport mechanism near the surface is usually diffusion as the flow velocities are low near the surface.

Possible adsorbate–adsorbate interaction at higher coverages and the influence of readsorbed products sometimes make it doubtful to use the same rate constants as obtained in UHV experiments.

Another important question is if radicals or products desorbed from the catalyst surface can initiate gas phase reactions that affect the overall kinetics. Evidence of such hetero–homogeneous reactions has been reported by Daniel *et al.* (20, 21) in the case of partial oxidation of propylene over bismuth molybdates and cuprous oxide. Oxidative coupling of methane is another example (3, 4). The role of the surface in such coupling reactions has been discussed by Xu *et al.* (22, 23).

To understand in detail the role of the surfaces in catalytic combustion and, more generally, in combustion near active surfaces, it is necessary to consider chemical reactions as well as gas and heat transport, both on the surface and in the gas phase. Radicals or heat from the surface can increase the gas phase reactivity due to heat release and radical desorption. The surface might also act in the reverse way, i.e. as a sink for radicals and heat produced in gas-phase reactions, thus inhibiting gas-phase reactions. Some of these effects, important for high temperature catalysis and cata lytically stabilized thermal (CST) combustors, were early studied experimentally by Cattolica and Schefer (24) and later by Pfefferle *et al.* (25–27), Griffin (28), and Markatou *et al.* (29, 30). They used imaging of OH and O concentrations outside a sample to determine the influence of a catalytic surface on gas-phase ignition in hydrogen/air, methane/air, and ethane/air systems. Griffin (28) pointed out that they were not able to unequivocally determine the mechanism of the observed catalytic promotion due to the influence of gas-phase reactions.

Markatou *et al.* (29) simulated some of the water formation experiments using a computer model that solves the conservation of mass, momentum, energy, and chemical species. The influence of the surface was modeled by applying a mass transport limited surface reaction, where the relative amounts of desorbed H_2O and OH were taken from published experimental data (7) from our group. The overall surface mechanism Markatou *et al.* used for determining the desorption of OH and H_2O assumed that the OH desorption rate amounts to 1/6 of the water desorption rate, which appears unreasonably high and the reference cited does not support this value. With the assumption of a very high OH desorption rate, Markatou *et al.* found that the majority of the OH radicals desorbed from the surface react with each other to form water and oxygen atoms. Their assumption of a high OH desorption rate is the likely reason that this path was found to be the dominating reaction for OH removal in the gas phase. The only parameter in our model that can be readily changed to affect the OH desorption rate is the preexponential for OH desorption. Based on our experimental estimates we used the value 10^{11}, and with this value the simulations give an OH desorption rate of 1/50,000 of the water desorption rate. A value of 10^{11} appears low but in order to obtain the OH/water desorption balance 1/6 as proposed by Markatou *et al.* it is necessary to increase the preexponential to 10^{15} which appears too high.

Ikeda *et al.* (31) used mass-spectrometry to analyze the hydrogen, oxygen, and water gradients in a stagnation flow of H_2 and O_2 impinging on a heated platinum surface. They compared their results to an analytic model which described the surface reactions and the transport in the gas. From these experiments they concluded that the activation energy for the surface oxidation step $H + OH = H_2O$ is lower at high surface coverages at atmospheric pressure than in the low coverage limit. No gas phase mechanism was included in the analytic model.

Several papers have been published exploring the variation of OH radical concentrations outside catalytically active surfaces at different temperatures and gas mixtures, in the low pressure regime, where the chemical interaction of desorbed OH with the surrounding gas can be neglected and where no OH is produced in the gas phase. Such data have been compared with kinetic models describing the surface reactions for pressures <0.2 torr, where the interaction with the surrounding gas is weak or negligible (7–9, 11) or can be handled by arranging the experiment in a proper way (14). These models have thus not included reactive gas phase processes.

Probing of desorbed OH radicals in catalyzed reactions involving O_2 and H_2 or hydrocarbons, respectively, has over the past decade been shown to be an efficient method for gaining knowledge both about surface catalyzed reactions and about combined surface and gas phase reactions (24–30). In our groups extensive studies (7–16) have been performed on the $H_2 + O_2$ reaction on Pt, complementing those of others studying the same reaction (19, 32–37). In these experiments a flow of reactants, such as H_2 and O_2, is directed onto a model catalyst, in the form of a polycrystalline foil or single crystal, which is resistively heated to temperatures above 1000 K. A small fraction of the intermediate OH radicals, produced in the catalytic oxidation of hydrogen to water at high temperature, desorbs and is detected, and in some cases spatially resolved (11, 14) with laser-induced fluorescence, LIF, outside the catalyst. The yield of water can at the same time be determined from the released chemical energy using calorimetry (7). These data have been interpreted by computer simulations based on kinetic models in which only surface reactions are included (8, 9, 17). This type of investigation has so far in most cases been limited to pressures below the viscous flow regime, i.e. in the molecular and intermediate pressure regimes below 0.2 torr, to avoid interference from the surrounding gas and mass transport limitation in the gas phase of the catalytic reaction.

METHODS

Experimental Setup

A schematic overview of the experimental set up is shown in Fig. 2. The vacuum system consists of a root pumped (max. pumping speed 75 L/s) stainless steel vacuum chamber. The reactant gases enter the chamber via a tube, 20 mm in diameter and 500 mm long, which ends 30 mm below the sample, resulting in a directed gas flow towards the surface. The flow of O_2 and H_2 was controlled by mass flow meters calibrated to give volume flow. The pressure in the vacuum chamber was measured with a capacitance manometer and regulated with the valve to the root pump, which changes the pumping speed.

A platinum foil, purity 99.95%, with the dimensions 3.8 × 20 mm and thickness 0.025 mm was resistively heated to 1300 K. The surface temperature was measured by a four-point resistance measurement and kept constant by microcomputer control. The temperature measurement was checked using a Pt/Pt 10% Rh thermocouple welded to the back of the foil. The difference between the thermocouple and the resistance measurements was 7 K at 1300 K. By inspection it could, furthermore, be seen from the heat glow that the temperature was even across the probed zone.

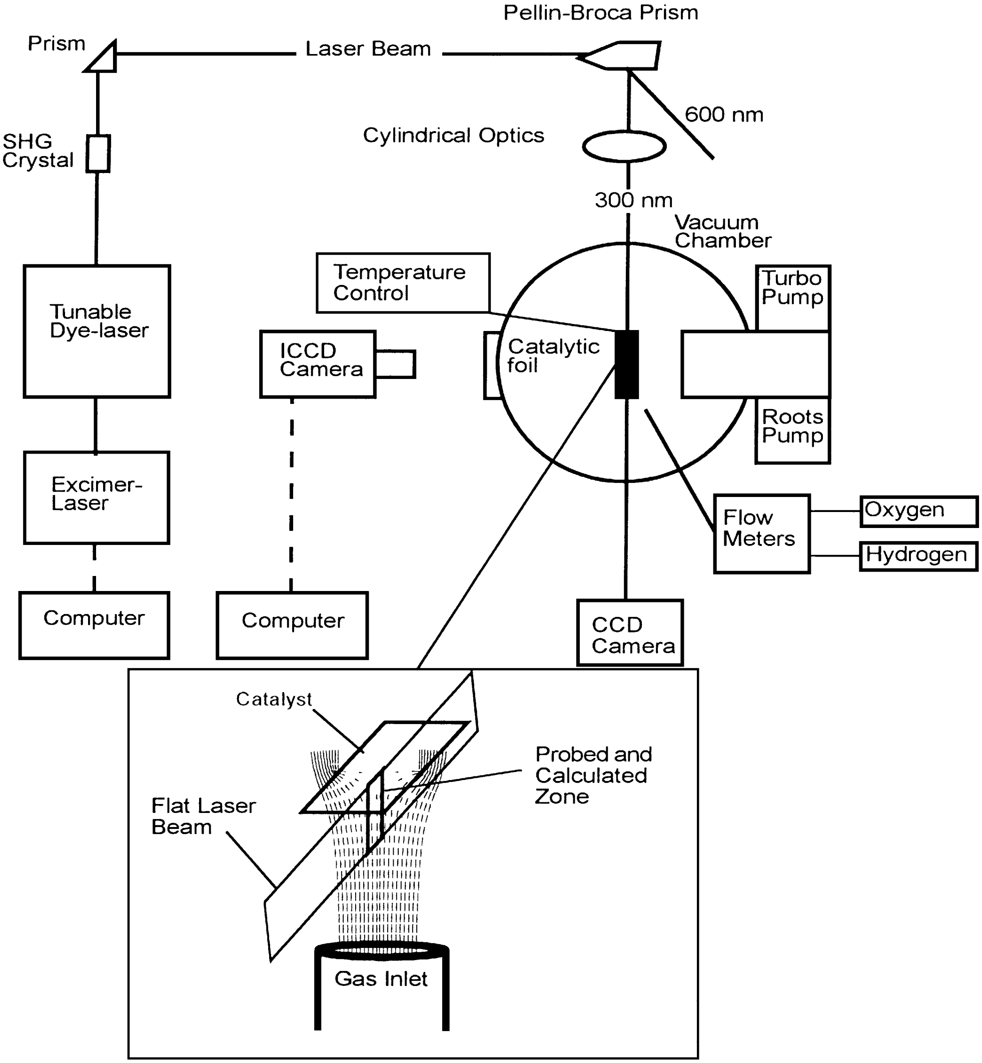

FIG. 2. Schematic view of the experimental setup. A stagnation flow of O_2 and H_2 impinges on a resistively heated platinum surface (3.8 × 20 mm). The distance between the tube and the surface is 30 mm. An UV laser sheet passes the center of the flow, making the OH molecules outside the surface fluoresce. The fluorescence light is imaged with a lens onto an image intensified charged coupled device, ICCD.

Before starting the measurements, the catalyst was run for 1 h at 1300 K in 10% H_2 and 90% O_2.

As the excitation light for probing of OH radicals we used the light from a frequency-doubled excimer-pumped dye laser (Lambda Physik EMG 102 E and FL 2002 E) in the wavelength region 306.3 to 307.5 nm, covering an absorption band of OH ($A^2\Sigma(\nu'=0)-X^2\Pi(\nu''=0)$). The laser pulses had a pulse length of 20 ns and a bandwidth of 0.2 cm^{-1}. The laser beam was shaped in the form of a sheet (10 mm × 0.1 mm) in the probed region outside the catalyst using cylindrical lenses and a telescope. Radiation from the heated platinum foil and stray light were eliminated with a bandpass filter (Schott UG 11). The laser beam was attenuated to a level where the recorded fluorescence was linear with the laser beam intensity over the entire image for the rotational line with the highest transition probability used.

The fluorescence light was imaged with a standard lens (Nikon UV quartz 4.5, f = 105 mm) mounted with a bellow extender for higher magnification on a gateable intensified charge coupled device (ICCD) camera (Princeton Instruments). The laser beam profile was recorded as it exited the chamber on a thermoelectrically cooled charge-coupled device (TE/CCD) camera (Princeton Instruments), and the profiles were used to normalize each fluorescence image.

Simulation of the Experiment

The mechanism describing the chemistry in the gas is shown in Table 1. The rate of a reaction is given by the Arrhenius expression:

$$AT^b\ e^{-E/kT},$$

where A is the preexponential, b is the temperature exponent, and E the activation energy for the reaction. The parameters for the gas phase chemistry are relatively well known and can be found in (5).

TABLE 1

Gas Phase Reactions Describing the Oxidation of Hydrogen

	Reaction	A	b	E (kJ/mol)
1	$O_2 + H = OH + O$	$2.0 \cdot 10^{14}$	0.0	70.3
2	$H_2 + O = OH + H$	$5.0 \cdot 10^{4}$	2.7	26.3
3	$H_2 + OH = H_2O + H$	$1.0 \cdot 10^{8}$	1.6	13.8
4	$OH + OH = H_2O + O$	$1.5 \cdot 10^{9}$	1.14	4.2
5	$H + H + M = H_2 + M$	$1.8 \cdot 10^{18}$	−1.0	0
6	$O + O + M = O_2 + M$	$2.9 \cdot 10^{17}$	−1.0	0
7	$H + OH + M = H_2O + M$	$2.2 \cdot 10^{22}$	−2.0	0
8	$H + O_2 + M = HO_2 + M$	$2.3 \cdot 10^{18}$	−0.8	0
9	$HO_2 + H = OH + OH$	$1.5 \cdot 10^{14}$	0.0	4.2
10	$HO_2 + H = H_2 + O_2$	$2.5 \cdot 10^{13}$	0.0	2.9
11	$HO_2 + H = H_2O + O_2$	$3.0 \cdot 10^{13}$	0.0	7.2
12	$HO_2 + O = OH + O$	$1.8 \cdot 10^{13}$	0.0	−1.7
13	$HO_2 + OH = H_2O + O_2$	$6.0 \cdot 10^{13}$	0.0	0
14	$HO_2 + HO_2 = H_2O_2 + O_2$	$2.5 \cdot 10^{11}$	0.0	−5.2
15	$OH + OH + M = H_2O_2 + M$	$3.3 \cdot 10^{22}$	−2.0	0
16	$H_2O_2 + H = H_2 + HO_2$	$1.7 \cdot 10^{12}$	0.0	15.7
17	$H_2O_2 + H = H_2O + OH$	$1.0 \cdot 10^{13}$	0.0	1.5
18	$H_2O_2 + O = OH + HO_2$	$2.8 \cdot 10^{13}$	0.0	26.8
19	$H_2O_2 + OH = H_2O + HO_2$	$5.4 \cdot 10^{12}$	0.0	4.2

TABLE 2

Surface Reactions Describing the Oxidation of Hydrogen on a Pt Surface

Reaction	A	E (eV)	S0	f(θ)
Adsorption/desorption of reactants				
$H_2 + 2Pt(s) \rightarrow 2H(s)$	-	-	0.046	$(1-\theta)$
$2H(s) \rightarrow H_2 + 2Pt(s)$	$3.7 \cdot 10^{21}$	0.7		
$O_2 + 2Pt(s) \rightarrow 2O(s)$	-	-	0.023	$(1-\theta)^2$
$2O(s) \rightarrow O_2 + 2Pt(s)$	$3.7 \cdot 10^{21}$	2.2	-	-
Surface reactions				
$H(s) + O(s) = OH(s) + Pt(s)$	$3.7 \cdot 10^{21}$	0.12	-	-
$H(s) + OH(s) = H_2O(s) + Pt(s)$	$3.7 \cdot 10^{21}$	0.18	-	-
$OH(s) + OH(s) = H_2O(s) + O(s)$	$3.7 \cdot 10^{21}$	0.5	-	-
Adsorption/desorption of products				
$H_2O + Pt(s) \rightarrow H_2O(s)$	-	-	0.75	$(1-\theta)$
$H_2O(s) \rightarrow H_2O + Pt(s)$	$1.0 \cdot 10^{13}$	0.44	-	-
$OH + Pt(s) \rightarrow OH(s)$	-	-	1	-
$OH(s) \rightarrow OH + Pt(s)$	$1.0 \cdot 10^{11}$	2.0	-	-
$O + Pt(s) \rightarrow O(s)$	-	-	1	$(1-\theta)$
$O(s) \rightarrow O + Pt(s)$	$1.0 \cdot 10^{13}$	3.8	-	-
$H + Pt(s) \rightarrow H(s)$	-	-	1	$(1-\theta)$
$H(s) \rightarrow H + Pt(s)$	$1.0 \cdot 10^{13}$	2.6	-	-

Table 2 shows the mechanism used for the surface chemistry. The rate of a reaction is given as an Arrhenius expression. However, for the surface chemistry all temperature exponents are set to zero. In general the surface phase mechanism is less known than the gas phase mechanism. For the adsorption reactions, characterized by a sticking coefficient at zero coverage, S_0, the rate of a reaction is given by the expression (38)

$$\frac{S}{1-S/2}\frac{1}{\Gamma^m}\sqrt{\frac{RT}{2\pi M}},$$

where S is the sticking coefficient at the actual coverage, Γ is the surface site concentration, m is the number of Pt atoms that will be covered in the reaction, R is the gas constant, T is the temperature, and M is the molecular weight of the considered molecule. The coverage dependence of the sticking coefficient is given in the rightmost column of Table 2. Thus the sticking coefficient at a certain coverage θ is given by $S = S_0\, f(\theta)$.

The surface mechanism is developed by Hellsing *et al.* (8, 9, 17). Values of the desorption energies for O and H were calculated from the enthalpy diagram given by Hellsing *et al.* (17). The preexponentials for desorption and the sticking coefficients of O, H, and OH are issues discussed in the next section.

We have used a computer model to simulate the stagnation flow impinging on a platinum catalyst. The SPIN code, developed by Coltrin *et al.* (39) is designed to solve the stationary problem. SPIN runs in conjunction with the CHEMKIN (40), SURFACE CHEMKIN (38), and TRANSPORT (41) packages, where the details of the reaction rate and transport property formulation can be found. SPIN uses TWOPNT solver (42) that implements a Newton/Time step algorithm (43) to obtain the steady state solution. Thermochemical properties for the gas-phase species were taken from the CHEMKIN thermodynamic database. The model accounts for finite-rate gas-phase and surface kinetics, and multicomponent molecular transport. It computes species and velocity profiles, and fluxes at the gas-surface interface, as well as surface coverage. The gas phase temperature can either be calculated or given as input as a measured temperature profile. If the temperature is calculated it is assumed that the heat exchange at the gas–surface interface is so efficient that the gas near the surface is of the same temperature as the surface. This is, however, not true at low pressures, where a temperature jump is present (44–46).

Flow Field Modeling

In the computer model it is assumed that we have an infinite surface, and an infinitely wide gas inlet with parallel flow lines at the inlet, which is illustrated in the right part of Fig. 3. The flow conditions of the experimental arrangement

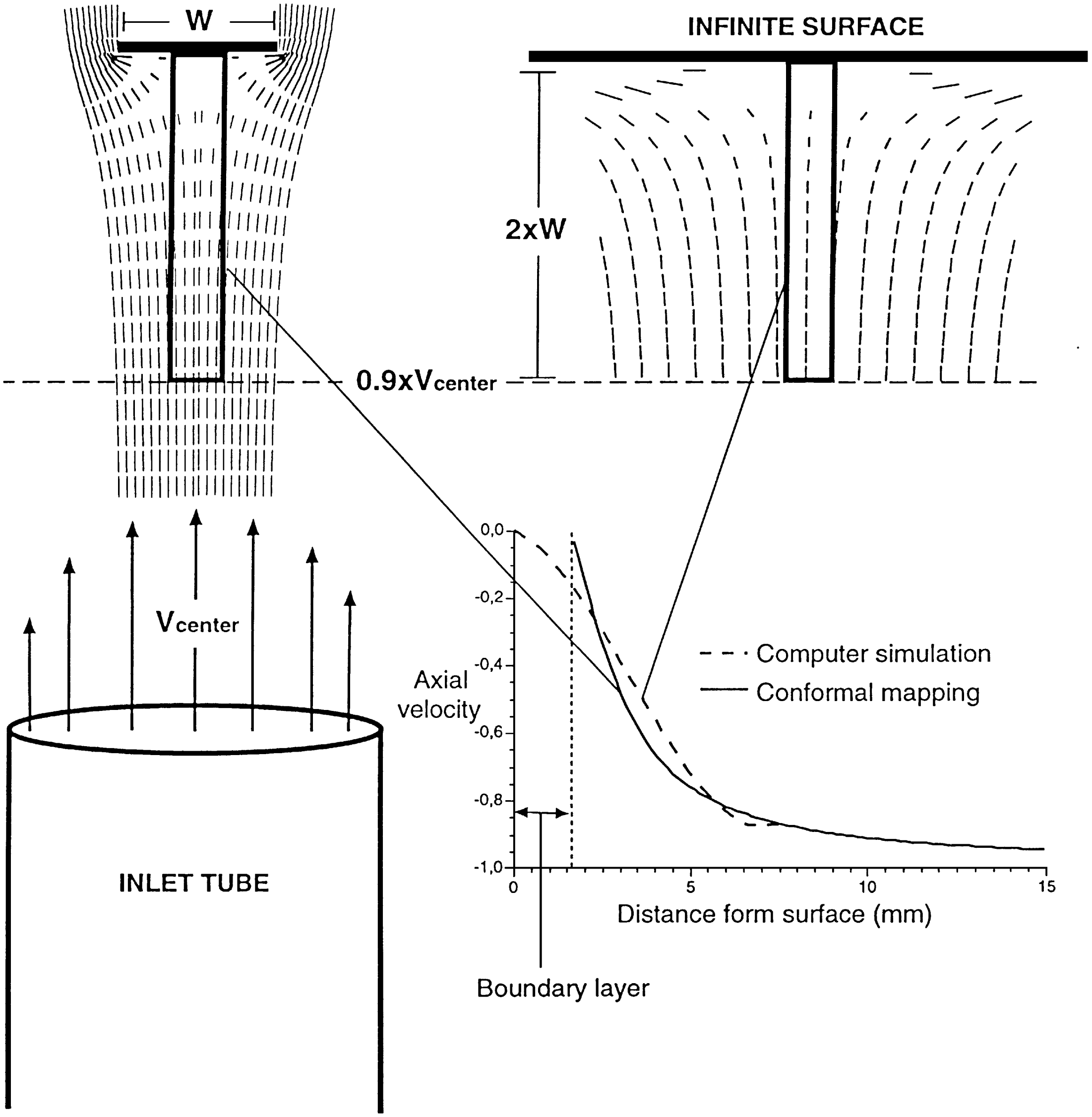

FIG. 3. Model system and experimental system with a graph showing the axial velocity profiles for the flow impinging on a strip calculated with conformal mapping and the flow calculated with a computer model.

are not as symmetric and therefore we have adopted a special approach to connecting the flow conditions of the experiment with those of the computer model.

In the experiment we use a 3.8 mm wide, 20 mm long strip, positioned 30 mm from the gas inlet, illustrated in the left part of Fig. 3. We thus need to establish which part of this flow can be considered to be a stagnation flow. In order to do this we calculate the flow field of an inviscid gas around a long thin strip using conformal mapping. The effect of viscosity is included by adding a boundary layer. The thickness of the boundary layer was calculated from the radial velocity in the stagnation flow of the computer model based on the standard definition of boundary layer thickness given in textbooks on flow field modeling, e.g. (47).

We use the flow velocity towards the surface, the axial velocity, as a criterion for similarity of flow fields between the more realistic flow field calculated with conformal mapping and the computer model. The comparison is shown in the lower right part of Fig. 3.

We find good agreement in the computer simulation if the distance between the gas inlet and catalytic surface is set to twice the width of the strip and the inlet velocity is set to 90% of the velocity far from the surface. The axial velocity agreement remained when the computer simulation was done with different gas compositions, temperatures, and pressures. The axial velocity of the conformal mapping calculation varies less than 10% in the central 1/4 of the strip width. Furthermore, variations of the inlet velocity in the model do not appreciably affect the results. For example, a 10% change of the inlet velocity gives a maximum change of less than 0.04 in the OH profiles of Fig. 5 (in normalized units), small enough not to affect our conclusions.

The most important difference between the conformal mapping calculation and the computer simulation is that the conformal mapping calculation simulates a purely two-dimensional flow while the computer model describes a radially symmetric situation. However, close to the center the radial velocity is in both systems very low and it does not affect the convective and diffusive transport. The parameters determining the mass transport are the much greater axial velocity, the temperature, and the gas composition.

The flow velocity far from the surface in the experimental system was assumed to be the central velocity of a long tube, i.e. twice the mean velocity in the tube, which is illustrated in the lower left part of Fig. 3. The mean velocity is given by the mass flow meters.

RESULTS AND DISCUSSION

In all the measurements presented here the surface temperature has been kept at 1300 K and the total gas flow at 800 SCCM, with 720 SCCM oxygen and 80 SCCM hydrogen. One SCCM (Standard Cubic CentiMeter) is equal to 4.08×10^{17} molecules/s at room temperature. The corresponding flow velocities at the center of the gas inlet were 64.4 m/s at 1 torr, 12.2 m/s at 5 torr, and 6.44 m/s at 10 torr. These conditions correspond to large oxygen excess from a gas phase stoichiometric point of view, and a slight oxygen excess from a surface kinetics point of view, at gradient free conditions. With gradients the oxygen excess at the surface increases. The difference between surface and gas phase stoichiometry is due to the higher sticking coefficient for H_2 compared to O_2.

The temperature profiles outside the Pt foil are rotational temperatures of OH calculated from fluorescence images recorded with the laser tuned to different rotational transitions. The measured rotational temperatures for the 1 torr case are shown in Fig. 4. The temperature profiles for the 5 and 10 torr cases were similar. These measured temperature profiles were used as input values in the simulations.

The $R_1(4)$ rotational transition was used to measure the OH concentration profiles, because its population is not sensitive to temperature variations within the range 300–1300 K. Quenching has to be taken into account to correctly relate the measured OH fluorescence with the OH concentration. The quenching of the OH molecules depends on local temperature and gas composition. Both these factors vary in the environment outside the catalyst. Therefore we measured the spatial variation of the lifetime outside the catalyst for the different reaction conditions. The lifetimes were measured by recording fluorescence images with different delays after the laser pulse and fitting the intensity in each pixel to an exponential. We found that the lifetimes decrease almost linearly away from the surface. The obtained lifetimes were in the 1 torr case 285 ns at 0.2 mm and 205 ns at 5 mm from the surface, in the 5 torr case 85 ns at 0.2 mm and 59 ns at 5 mm from the surface, and in the 10 torr case 50 ns at 0.2 mm and 32 ns at 5 mm from the surface. Comparing these results with lifetimes calculated from quenching cross sections given by Fairchild *et al.* (48) we conclude that the change in lifetime with distance from the surface is due to the temperature gradient present outside the surface, which gives a variation in both gas density and collisional energy at different positions outside the surface.

The measured quenching-corrected relative OH concentrations are shown, together with the calculated profiles, for the pressures 1, 5, and 10 torr in Figs. 5a, b, and c. The simulations were performed both with and without the gas phase mechanism. The calculated and the measured profiles are all normalized to unity at 0.2 mm from the surface.

The form of the OH profile is not influenced at all by gas phase reactions at 1 torr pressure (Fig. 5a). Consequently, the surface reaction kinetics dominate at this and lower pressures. Note that this conclusion applies in the case of a reactive gas phase species (OH). The shape of the profile in Fig. 5a is mainly dependent on the magnitude of the

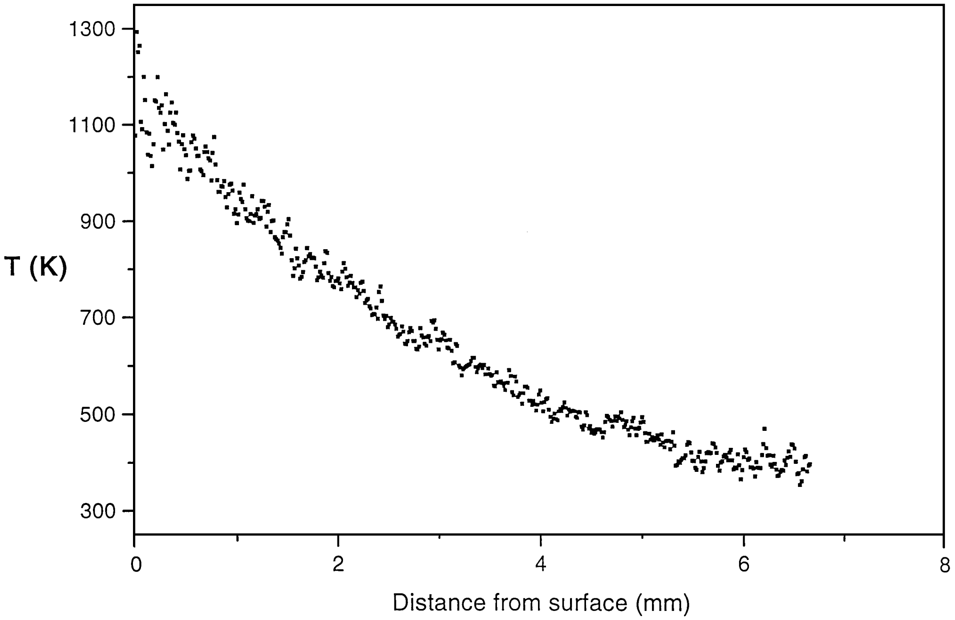

FIG. 4. Measured rotational temperature vs distance from the surface at 1 torr.

flow velocity, since the OH radicals are removed from the region outside the surface by convection and diffusion, not by reactions.

For higher pressure the gas phase chemistry becomes increasingly more important. In Figs. 5b and c there is a significant difference between the simulations with and without gas phase chemistry. Without gas phase reactions the OH concentration falls off too slowly, compared to the experimental results. Inclusion of the gas phase reactions provides a correction in the right direction but seems to slightly overestimate the gas phase consumption of OH. From simulations we also find that the curve shape is less sensitive to the flow velocity at higher pressures, reflecting that the reactive consumption of OH becomes increasingly more important as the pressure increases.

Gas Phase Chemistry

At the present reaction conditions OH is the only radical species significantly desorbed from the surface; i.e., H and O desorption are not of first-order importance. The gas phase chemistry can be approximated as consisting of the reaction chain initiated by the desorbed OH. If the OH desorption is turned off, the remaining radical production in the gas phase is negligible. In this sense desorption of OH molecules produced in the surface reactions is responsible for all the gas phase chemistry outside the catalyst.

Summarized below are the important gas-phase reaction steps involved in the consumption of gas phase OH at 10 torr. The sticking coefficient of OH is assumed to be unity; (s) denotes a surface species:

Consumption of OH originally desorbed from the surface:

$$OH \rightarrow OH(s) \quad 96\% \text{ (readsorption)} \qquad [1]$$

$$OH + H_2 \rightarrow H_2O + H \quad 4\%. \qquad [2]$$

Consumption of H produced by reaction [2]:

$$H \rightarrow H(s) \quad 84\% \qquad [3]$$

$$H + O_2 \rightarrow OH + O \quad 1\% \qquad [4]$$

$$H + O_2 + M \rightarrow HO_2 + M \quad 15\%. \qquad [5]$$

Consumption of O produced in reaction [4]:

$$O \rightarrow O(s) \quad 92\% \qquad [6]$$

$$O + H_2 \rightarrow OH + H \quad 8\%. \qquad [7]$$

The absolute values of the OH concentrations in Fig. 5 are sharply influenced by the OH sticking coefficient. If a sticking probability smaller than 1 is assumed, the absolute OH concentration increases, but the shape of the simulated profiles in Fig. 5 does not change. If the sticking coefficient of OH is set to 0 the OH concentration becomes 27 times higher close to the surface, compared to a sticking coefficient of 1. It is, however, difficult to rationalize a sticking coefficient much less than unity for a reactive radical on a surface where it is known to bind strongly. For this reason a sticking coefficient of 1.0 has been used for the O, H, and OH radicals. This choice of parameter values has also been adopted in (49, 50).

The faster falloff of the OH profiles seen at 5 and 10 torr pressure is due to reaction [2]; i.e., OH is consumed through the gas phase reaction $H_2 + OH \rightarrow H_2O + H$.

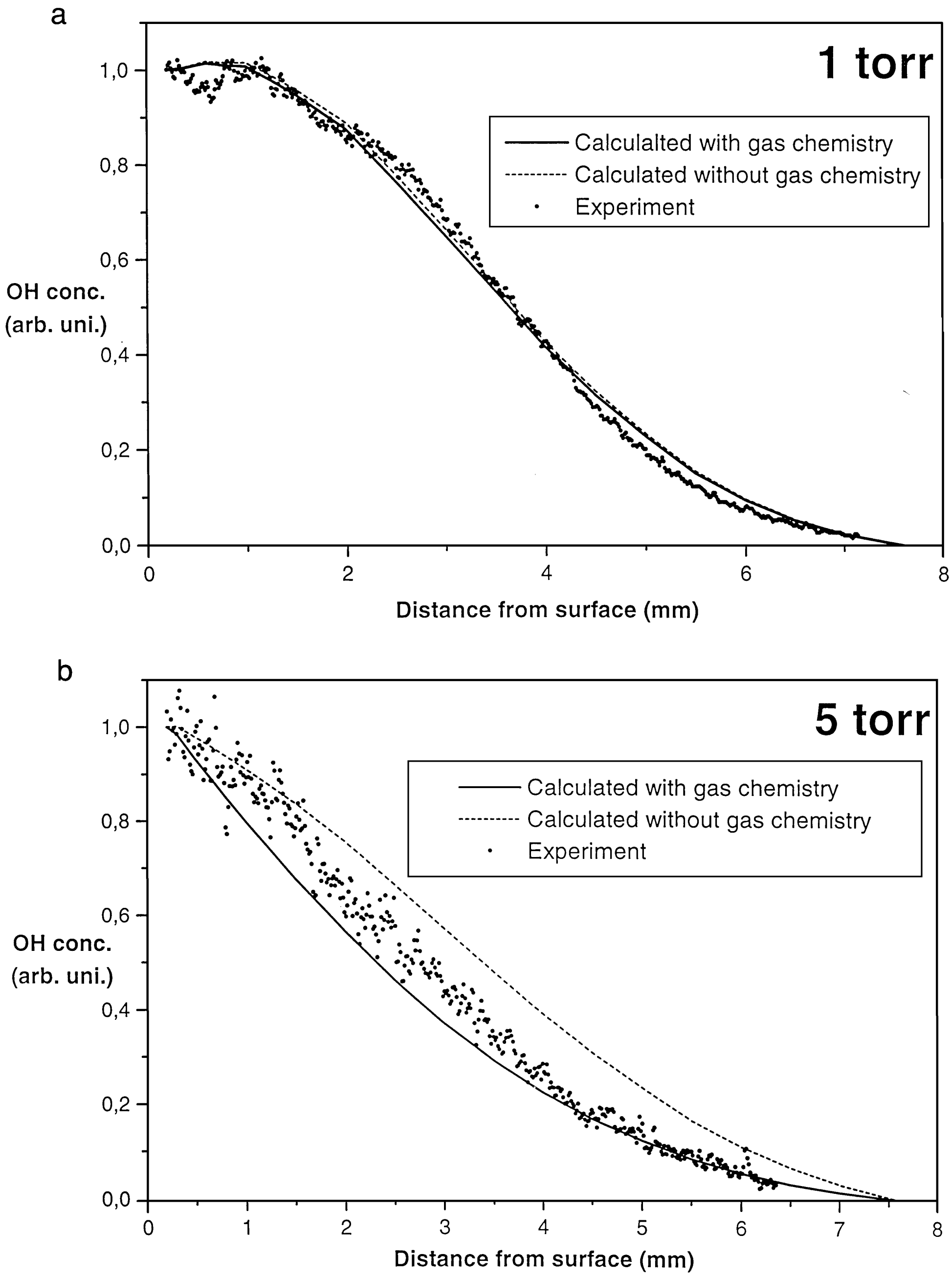

FIG. 5. Measured and calculated relative OH concentration profiles vs distance at 1, 5, and 10 torr. The measured profiles have been corrected for intensity variations in the laser sheet. The measured and calculated profiles are set to the same value at 1 mm from the surface. The unbroken line is the result from calculations done with reactive gas-phase chemistry. The broken line is the result from calculation done with nonreactive gas-phase chemistry.

Most of the H atoms produced are then removed from the gas phase by sticking on the surface. The sticking coefficient of atomic hydrogen is set to 1, reaction [3], which is quite reasonable, considering the high reactivity of H and relatively strong bonding of H on Pt. The majority of the remaining H atoms are consumed in the reaction $H + O_2 + M \rightarrow HO_2 + M$, where M is a third body (reaction [5]). Almost all of the HO_2 molecules are consumed in the reaction $HO_2 + OH \rightarrow H_2O + O_2$. Only a small fraction of the H atoms reacts with O_2 to form atomic oxygen and OH, reaction [4]. Just as for OH and H, most of the produced oxygen atoms adsorb onto the surface since the sticking coefficient for atomic oxygen is set to 1 in the simulation, also quite reasonably, with the same arguments as for H and OH. The remaining oxygen reacts with hydrogen to form H atoms and OH, continuing the chain reaction [7].

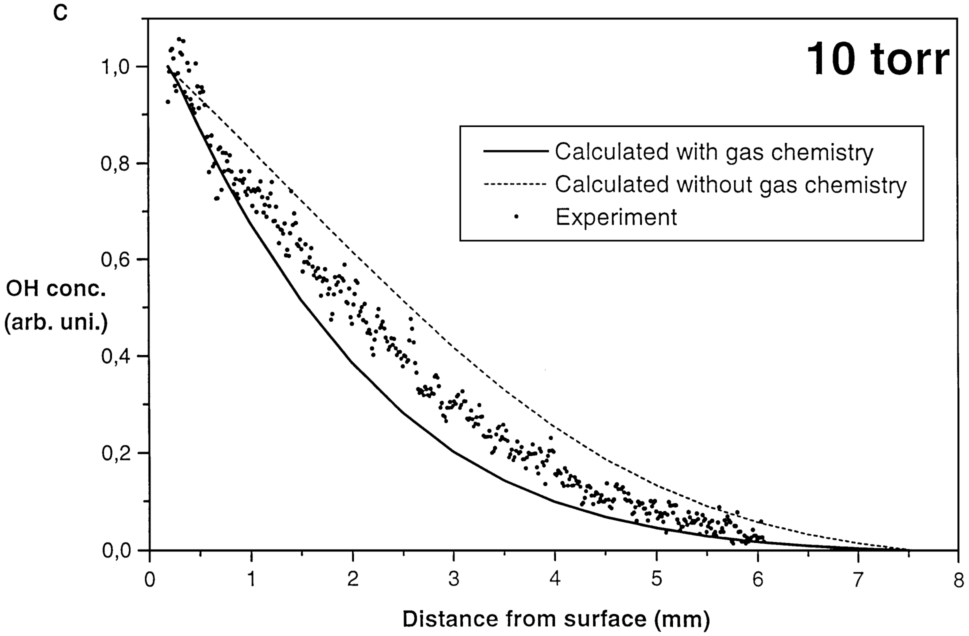

FIG. 5—*Continued*

A few other reactions also take place but these consume <1% of the radicals.

In this reaction scheme, reactions [4] and [7] are chain-branching reactions that could lead to gas phase ignition, but under the conditions studied here the amount of hydrogen atoms present was never enough to cause ignition at the gas temperatures used in the simulation. With higher pressure, gas phase temperatures, or more H atoms present, the simulation would most likely produce a gas phase ignition.

In the simulations one also finds the onset of mass transport limitation; the relative hydrogen pressure near the surface decreases if the pressure is increased and if the flow velocity is decreased. At the inlet the gas mixture contains 10% hydrogen but at the surface the hydrogen concentrations are 9%, 4%, and 3% at 1, 5, and 10 torr, respectively.

A different reaction path for removal of surface-generated OH has been suggested by Markatou *et al.* (29) in a comparable simulation at atmospheric pressure. They found the main reaction path to be a recombination of OH molecules. This was based on a very high OH desorption rate which resulted in a high probability of collisions between OH molecules. The OH desorption rate in (29) was assumed to be only 6 times lower than the water desorption rate. This rate is much too high, according to our previous work (7).

Surface Chemistry

As noted above, the form of the calculated OH concentration profiles in Fig. 5 does not depend on the sticking coefficient of OH. Only the absolute values of the OH concentrations are changed when the sticking coefficient is varied. A crude estimate of the OH concentration can be done from the measured LIF intensity, taking into account the laser intensity and the detection efficiency of the optics and the CCD camera. This gives an experimental estimate OH concentration of $4 \times 10^{10\pm1}$ OH molecules/cm^3 at 1 torr, 1 mm from the surface. In the simulation the same OH concentration is obtained if the preexponential for OH desorption is set to 10^{11}, together with the sticking coefficient 1. Calculations with a higher preexponential give a higher OH concentration outside the surface, but still the same shape of the concentration profiles, and the same chemistry since the chain reaction does not propagate substantially further from Eq. [2], $OH + H_2 \rightarrow H_2O + H$, as the amount of atomic hydrogen is not enough to cause ignition at the gas temperatures used in the simulation.

The preexponentials for the H and O desorption were found to be relatively unimportant since the high activation energy for O-desorption and the low coverage of hydrogen (due to the large O_2 excess) inhibit significant desorption of O and H atoms at 1300 K.

CONCLUSIONS AND SUMMARY

Experimental measurements and simulations have been performed of OH concentration profiles outside a Pt catalyst, producing and consuming OH radicals. We conclude that the dominant fraction of OH present outside the catalytic surface is formed on the surface and not in gas-phase reactions for pressures up to 10 torr. This implies that the variations in OH concentration in the gas phase outside a catalyst can be used to probe the surface mechanism at pressures <10 torr, provided the influence of diffusion, convection, and gas-phase chemistry is taken into account in the simulations.

We have specially found that the measured OH concentrations at 1 torr are governed entirely by surface kinetics and transport, i.e. diffusion and convection, and not by gas-phase reactions. At 5 and 10 Torr it is necessary to include chemical reactions in the gas phase because the desorbed OH radicals here react with hydrogen, constituting a significant consumption path of OH. This is a different reaction path for the removal of surface-generated OH than was assumed in a comparable simulation at atmospheric pressure (29). The results provide a basis for extension of this type of studies to higher pressures, where the gas-phase kinetics become more important.

ACKNOWLEDGMENTS

We gratefully acknowledge financial support from Volvo Research Foundation and Volvo Educational Foundation (Contract 92 : 36), the Swedish Natural Science Research Council (NFR, Contract E-EG 2560-129), the Swedish Research Council for Engineering Sciences (TFR, Contract 92-538), and the Swedish Institute (SI). One of us (F.B.) gratefully acknowledges the financial support by the Deutsche Forschungsgemeinschaft for a one-year stay at Chalmers University of Technology. Two of us, JLP and MF, gratefully acknowledge support from the Combustion Engine Research Center (CERC).

REFERENCES

1. Hayes, R. E., and Kolaczkowski, S. T., “Introduction to Catalytic Combustion,” Gordon & Breach Science, Amsterdam, 1997.
2. Warnatz, J., Maas, U., and Dibble, R. W., “Combustion,” Springer-Verlag, Berlin, 1995.
3. Peng, X. D., and Stair, P. C., *J. Catal.* **128**, 264 (1991).
4. Wang, J. X., Driscoll, D. J., and Lunsford, J. H., *J. Catal.* **112**, 366 (1988).
5. Baulch, D. L., Cox, R. A., Just, T., Kerr, J. A., Pilling, M. J., Troe, J., Walker, R. W., and Warnatz, J., *J. Phys. Chem. Ref. Data* **21**, 411 (1992).
6. Hellsing, B., Kasemo, B., and Zhdanov, V. P., *J. Catal.* **132**, 210 (1991).
7. Ljungström, S., Kasemo, B., Rosén, A., Wahnström, T., and Fridell, E., *Surf. Sci.* **216**, 63 (1989).
8. Hellsing, B., Kasemo, B., Ljungström, S., Rosén, A., and Wahnström, T., *Surf. Sci.* **189/190**, 851 (1988).
9. Wahnström, T., Fridell, E., Ljungström, S., Hellsing, B., Kasemo, B., and Rosén, A., *Surf. Sci.* **223**, L905 (1989).
10. Wahnström, T., Ljungström, S., Rosén, A., and Kasemo, B., *Surf. Sci.* **234**, 439 (1990).
11. Fridell, E., Westblom, U., Aldén, M., and Rosén, A., *J. Catal.* **128**, 92 (1991).
12. Fridell, E., Hellsing, B., Kasemo, B., Ljungström, S., Rosén, A., and Wahnström, T., *J. Vac. Sci. Technol. A* **9**, 2322 (1991).
13. Fridell, E., *Chem. Phys. Lett.* **188**, 487 (1992).
14. Gudmundson, F., Fridell, E., Rosén, A., and Kasemo, B., *J. Phys. Chem.* **97**, 12828 (1993).
15. Fridell, E., Kasemo, B., and Rosén, A., *Langmuir* **110**, 699 (1994).
16. Fridell, E., Elg, A-P., Rosén, A., and Kasemo, B., *J. Chem. Phys.* **102**(14), 5827 (1995).
17. Fassihi, M., Zhadanov, V. P., Rinnemo, M., Keck, K-E., and Kasemo, B., *J. Catal.* **141**, 438 (1993).
18. Försth, M., Persson, J. L., Gudmundson, F., and Rosén, A., The influence of a catalytic surface on the gas phase ignition and combustion of $H_2 + O_2$, to be published.
19. Anton, A. B., and Cadogan, D. C., *J. Vac. Sci. Technol. A* **9**, 1890 (1991).
20. Daniel, C., and Keulks, G. W., *J. Catal.* **24**, 529 (1972).
21. Daniel, C., Monnier, J. R., and Keulks, G. W., *J. Catal.* **31**, 360 (1973).
22. Xu, M., and Lunsford, J. H., *J. Chem. Soc., Chem. Commun.*, 1203 (1995).
23. Xu, M., Ballinger, T. H., and Lunsford, J. H., *J. Phys. Chem.* **99**, 14494 (1995).
24. Cattolica, R. J., and Schefer, R. W., The effect of surface chemistry on the development of the [OH] in a combustion boundary layer, *in* “Nineteenth Symposium (International) on Combustion,” p. 311, Combustion Inst., Pittsburgh, 1982.
25. Pfefferle, L. D., Griffin, T. A., and Winter, M., *Appl. Opt.* **27**(15), 3197 (1988).
26. Pfefferle, L. D., Griffin, T. A., Winter, M., Dyer, M. J., and Crosley, D. R., *Combust. & Flame* **76**, 325 (1989).
27. Pfefferle, L. D., Griffin, T. A., Winter, M., Dyer, M. J., and Crosley, D. R., *Combust. & Flame* **76**, 339 (1989).
28. Griffin, T. A., Ph.D. thesis, Yale University, 1991.
29. Markatou, P., Pfefferle, L. D., and Smooke, M. D., *Combust. Sci. Technol.* **79**, 247 (1991).
30. Markatou, P., Pfefferle, L. D., and Smooke, M. D., *Combust. & Flame* **93**, 185 (1993).
31. Ikeda, H., Sato, J., and Williams, F. A., *Surf. Sci.* **326**, 11 (1995).
32. Fischer, G. B., and Gland, J. L., *Surf. Sci.* **94**, 446 (1980).
33. Fischer, G. B., and Sexton, B., *Phys. Rev. Lett.* **44**, 683 (1980).
34. Fischer, G. B., Gland, J. L., and Schmeig, S. J., *J. Vac. Sci. Technol. A* **9**, 1890 (1991).
35. Germer, T. A., and Ho, W., *Chem. Phys. Lett.* **163**, 449 (1989).
36. Ogle, K. M., and White, J. M., *Surf. Sci.* **139**, 43 (1984).
37. Anton, A. B., and Cadogan, D. C., *Surf. Sci. Lett.* **239**, L548 (1990).
38. Coltrin, M. E., Kee, R. J., and Rupley, F. M., Sandia National Laboratories Report SAND83-8209, Sandia National Laboratories, Livermore, 1983.
39. Coltrin, M. E., Kee, R. J., Evans, G. H., Meeks, E., Rupley, F. M., and Grcar, J. F., Sandia National Laboratories Report SAND91-8003, Sandia National Laboratories, Livermore, 1991.
40. Kee, R. J., Rupley, F. M., and Miller, J. A., Sandia National Laboratories Report SAND90-8003B, Sandia National Laboratories, Livermore, 1991.
41. Kee, R. J., Dixon-Lewis, D., Warnatz, J., Coltrin, M. E., and Miller, J. A., Sandia National Laboratories Report SAND86-8246, Sandia National Laboratories, Livermore, 1991.
42. Grcar, J. F., Sandia National Laboratories Report SAND91-8230, Sandia National Laboratories, Livermore, 1991.
43. Grcar, J. F., *in* “Twenty-First Symposium (International) on Combustion,” p. 1773, Combustion Inst., Pittsburgh, 1986.
44. Smoluchowski, M., *Phil. Mag.* **46**, 192 (1898).
45. Kennard, E. H., “Kinetic Theory of Gases,” McGraw–Hill, New York/London, 1938.
46. Leyendecker, G., Doppelbauer, J., and Bäuerle, D., *Appl. Phys. A* **30**, 237 (1983).
47. Munson, B. R., “Fundamentals of Fluid Mechanics,” Wiley, New York, 1994.
48. Fairchild, P. W., Smith, G. P., and Crosley, D. R., *J. Chem. Phys.* **79**(4), 1795 (1983).
49. Rinnemo, M., Deutschmann, O., Behrendt, F., and Kasemo, B., *Combust. & Flame* **111**, 312 (1997).
50. Warnatz, J., Allendorf, M. D., Kee, R. J., and Coltrin, M. E., *Combust. & Flame* **96**, 393 (1994).